Atomic Force Spectroscopy in Biological Complex Formation: Strategies and Perspectives

ARTICLE *in* THE JOURNAL OF PHYSICAL CHEMISTRY B · NOVEMBER 2009

Impact Factor: 3.3 · DOI: 10.1021/jp902421r · Source: PubMed

2 AUTHORS:

Anna Rita Bizzarri
Tuscia University
116 PUBLICATIONS **2,354** CITATIONS
SEE PROFILE

Salvatore Cannistraro
Tuscia University
219 PUBLICATIONS **3,541** CITATIONS
SEE PROFILE

THE JOURNAL OF PHYSICAL CHEMISTRY B

 VOLUME 113, NUMBER 52, DECEMBER 31, 2009

FEATURE ARTICLE

Atomic Force Spectroscopy in Biological Complex Formation: Strategies and Perspectives

Anna Rita Bizzarri* and Salvatore Cannistraro

Biophysics and Nanoscience Centre, CNISM, Facoltà di Scienze, Università della Tuscia, Largo dell'Università, 01100 Viterbo, Italy

Received: March 18, 2009; Revised Manuscript Received: October 12, 2009

Atomic force spectroscopy has become a widely used technique for investigating forces, energies, and dynamics of biomolecular interactions. These studies provide dissociation kinetic parameters by pulling apart proteins involved in a complex. Biological complexes are studied under near-physiological conditions, without labeling procedures, and are probed one at time, the latter allowing to one obtain results which are not averaged over the ensemble. However, to gain reliable information, some experimental aspects have to be carefully controlled. In particular, the immobilization of molecular partners to AFM tips and supports, required to force the molecular dissociation, plays a crucial role in determining the success of the experiments. To actually resolve single interactions, multiple simultaneous complex dissociations have to be avoided, and nonspecific adhesions, commonly found in these studies, have to be recognized and discarded. This article is aimed at offering a critical revisitation of the atomic force spectroscopy technique applied to the study of biomolecular interactions, highlighting the critical points, identifying strategies to be adopted for a more reliable data extraction and interpretation, and pointing out the experimental and theoretical aspects which still need to be refined. To this purpose, we take advantage of the vast landscape of literature and then proceed into the details of our works. In this respect, we describe the general principles of the technique, the procedures for protein immobilization, and how they can affect the results. We emphasize the use of computational docking to predict molecular complex configurations, when unknown, as a useful approach to select proper anchorage architectures. Additionally, we deal with data acquirement and analysis, with regard to the force curve selection, to the force histograms interpretation, and to the theoretical frameworks used to extract kinetic parameters. Through this, we outline that AFS can be successfully used both to investigate complexes having very different affinities and also to reveal competitive binding mechanisms, thus gaining deeper information about molecular interactions.

Introduction

Since its early days, atomic force microscope (AFM) has proven to be a powerful tool for getting insight into nanometric objects, enabling scientists to investigate novel aspects, even at the level of single molecules. This new opportunity makes possible also the discovery of differences among molecules that would be otherwise undetectable by more conventional techniques, whose results are an average of ensemble measurements. The AFM is a high-resolution imaging tool using a very sharp tip located at the end of a cantilever spring; the tip is mounted on a piezoelectric stage which is able to ensure a three-

* To whom correspondence should be addressed. Phone: +39 0761 357031. Fax: +39 0761 357027. E-mail: bizzarri@unitus.it.

10.1021/jp902421r CCC: $40.75
Published on Web 11/11/2009

Anna Rita Bizzarri received her degree in Physics in 1987 from the University of Rome. She obtained a Ph.D in Biophysics in 1992 from SISSA in Trieste. After postdoctoral fellowships in Perugia and Mainz, she joined the Science Faculty, Tuscia University, Italy, as a Research Assistant. in 2000 she became Associate Professor of Physics, and in 2006 she obtained the position of Full Professor. Her scientific interests include spectroscopic investigations and MD simulations of electron-transfer metalloproteins. More recently, she is focused on single-molecule-level detection by surface enhanced raman spectroscopy and scanning probe microscopies for both fundamental and applicative aims.

Salvatore Cannistraro obtained his degree in Physics in 1972 from Pisa University. He received his Ph.D. in Biophysics at Liegi University, Belgium. In 1977, he became Reader of Biophysics at Calabria University. He moved to Perugia University on 1981 as Associate Professor of Molecular Physics. Since 1991, he has been a Professor of Physics, Biophysics and Nanoscience at Tuscia University, leading the Biophysics, Nanoscience Centre. His scientific interests regard optical, magnetic, and neutron spectroscopies and modeling of amorphous and biological systems. More recently, he is focusing his activity on the application of AFM, STM, and Raman SERS to single biomolecule detection and nanobiomedicine.

dimensional positioning with subnanometer resolution. The tip and sample feel the effects of interatomic forces that can be easily monitored by an optical detection system.

These characteristics make the AFM able to image nanostructures when the tip is scanned in the $x-y$ plane along the sample surface.[1−3] The AFM can operate also in fluid, and samples can be examined in near-physiological conditions, without labeling or altering procedures, and also at work. It is possible, for example, to observe biological activities such as the formation of specific complexes[4−7] or other biomolecular processes.[8,9]

In addition, the AFM cantilever can be used as a piconewton-sensitive probe for measuring inter- and intramolecular forces.[10−12] Atomic force spectroscopy (AFS) has been widely used by researchers in the latest years to study many different molecular properties and mechanisms such as polymers stretching,[13] cellular membrane elasticity,[14] protein unfolding,[15,16] and molecular interactions.[17−19] In these cases, the tip is moved along the vertical direction, pulling molecules apart to stretch, unfold, or separate them. To study the binding properties of two biomolecules, for example, one interacting partner is immobilized on a support while the other is anchored to the AFM tip. The functionalized tip is therefore brought into contact with the support, and a complex may be formed, provided that the two partners have enough flexibility and reorientational freedom. Successively, the tip is retracted from the substrate. When the applied external force overcomes the interaction forces, the tip jumps off sharply to a noncontact position, and dissociation takes place. Such a jump-off process provides an estimation of the unbinding force if the cantilever spring constant is known.[10−12]

Therefore, the dissociation is not spontaneous, but it is the tip that, moving back from the functionalized support, applies an external force which may lead the biomolecules to dissociate. The application of an external force to the biomolecules may alter the equilibrium energy landscape of the complex.[20] Thereby, the possibility of extracting kinetics and thermodynamics parameters from these nonequilibrium measurements requires the use of suitable theoretical models. The most widely used is that of Bell−Evans,[21,22] which allows one to derive the dissociation rate constant (k_{off}) and the width of the energy barrier (x_β), which are important parameters to describe the interaction process.

Given its ability to provide kinetic informationat the level of single molecule, AFS is unquestionably innovative. However, some issues concerning this technique certainly deserve attention. One of the key topics of AFS experiments is the immobilization strategy of the biological partners. To ensure an effective and iterative protein association−dissociation process, the biomolecules have to be stably tied to supports, but at the same time, they have to preserve their functionality and keep the binding site accessible to the counterpart. In this respect, the properties of the surfaces on which biomolecules are fastened can affect their structure as well as their coverage density.[23,24]

Single-molecule recognition studies require that interactions be probed one at a time. If multiple dissociations take place at the same time, they could be erroneously held as a single event and introduce some errors into the data analysis. A variety of strategies have been developed in order to better approach the detection of single unbinding events.[18,25]

Another nodal point is the occurrence of nonspecific interactions, which are always found in AFS experiments. To reduce their frequency, or at least to discriminate between them and specific unbinding events, different strategies have been developed. To such an aim, it is of common use to immobilize proteins by means of bifunctional flexible linking spacers.

Although the Bell−Evans model is still widely used, the emergence of some discrepancies in the measured dissociation rates from the unbinding of some ligand−receptor systems has led either to revise it or to develop new theoretical approaches for a better description of the related processes.[26−28]

In this work, we present a critical analysis of the force spectroscopy applied to biological complexes for the investigation of unbinding processes. We describe the technique by illustrating its principles and the strategies to prepare samples. We discuss the data analysis criteria related to the force curve selection, the force histograms, and the theoretical frameworks to extract the relevant kinetic parameters. These general concepts are then discussed within a more specific context by revisiting the studies that we have performed to investigate three different protein complexes, the bacterial transient azurin−cytochrome c551,[29,30] the heterologous p53−azurin,[19] and the human p53−Mdm2.[31] We get through these works describing, in particular, the adopted immobilization strategies, pointing out how they have affected the obtained results. Moreover, we emphasize the advantage of performing preliminary computational docking studies to identify the putative regions of the proteins involved in the interaction. Finally, we summarize the most reliable experimental and theoretical procedures, selected from the literature, with some hints to some possible new interesting future developments.

Molecular Recognition and Dynamic Force Spectroscopy

Molecular recognition is at the basis of life. Every biological process is carried out and regulated by numerous molecular associations and dissociations, each one inducing a distinct effect. The possibility of giving rise to all of the complexity of biological functions resides not only in the large number of molecules involved but also in the different character of their bindings. Protein interactions are governed by intermolecular forces and binding energies, which define their stability. As a consequence, the detailed knowledge of these factors is pivotal for understanding the nature of their association.

In general, biomolecular interactions can be described by the law of mass action. The formation of a complex between two partners, like a receptor R and a ligand L, at equilibrium, can be represented as

$$R + L \leftrightarrow RL \quad (1)$$

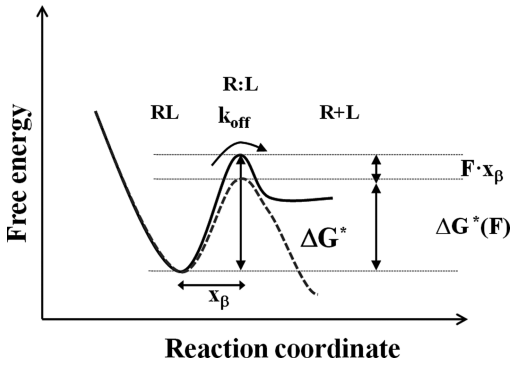

Figure 1. Energy profile for a dissociation process of a biomolecular complex at equilibrium (continuous line) and under the application of a force F (dashed line). ΔG^* is the activation free energy, x_β is the width of the energy barrier, and k_{off} is the dissociation rate.

and the law is commonly expressed as follow

$$[R][L]/[RL] = K_d = 1/K_a \quad (2)$$

where K_d and K_a represent the dissociation and association constants, respectively, which are indicative of the interaction affinity.

The kinetics of the reaction at equilibrium is given by

$$d[RL]/dt = k_{on}[R][L] - k_{off}[RL] = 0 \quad (3)$$

where k_{on} and k_{off} represent the association and dissociation rate constants, respectively. By comparing eqs 2 and 3, we obtain

$$K_a = k_{on}/k_{off} \quad (4)$$

The important consequence of this observation is that the same biomolecular affinity may correspond to different couples of k_{on} and k_{off} (and different couples of time scales $\tau_{on} = 1/k_{on}$ and $\tau_{off} = 1/k_{off}$).

Both the association and dissociation rate constants depend on the properties of the interaction (i.e., the distance, the shape, and electrostatic complementarity of the proteins at the binding interface) as well as on the environmental conditions (i.e., local concentration and diffusion of biomolecules and so forth). However, while k_{on} is mainly dominated by the diffusive properties, k_{off} is more strongly related to the number and strength of the bonds holding the proteins together.[32−34] The dissociation rate constant depends on the activation free energy $\Delta G^{\#}$ of the reaction, as shown in Figure 1, through

$$k_{off} = A \exp(-\Delta G^{\#}/k_B T) \quad (5)$$

where A is the Arrhenius prefactor, k_B is the Boltzmann constant, and T is the absolute temperature. It is thus clear that the knowledge of this parameter, related to the complex stability and lifetime, is quite important to gain insight into the characteristics of the interaction.

The dissociation rate of molecular interactions can be determined by various methods. Flow techniques, used to investigate relatively slow processes, and relaxation techniques, suitable also for faster reactions, are the mainly used approaches.[35] They follow the unbinding of molecules by monitoring changes in optical signals, such as fluorescence or absorbance, of marked specimens. In the latest years, a more and more frequent use of surface plasmon resonance to investigate the unbinding kinetics between receptors immobilized on special gold slides with a ligand solution flowed on them has been registered.[36] In this case, the molecules do not need to be marked, and low concentrations can be investigated. Although all of these approaches provide extensive kinetic details about the interaction of biomolecules, their results are an average of numerous molecules observed at the same time.

The strength of AFS is the ability to probe molecules one at time, so that the outcome of each single interaction is recorded. Given the high sensitivity of the technique, it enables one to put into evidence also possible inhomogeneities within a biological sample, revealing functional inequality of molecules (e.g., the presence of mutations in a biomolecule or the existence of different conformational states of the molecules[37,38]).

It has to be emphasized that AFS studies can characterize in detail the energy landscape of a complex dissociation, which is useful to understand the features of a specific interaction, such as the number, height, and the shape of energy barriers, the energy landscape, and the rate of the related transitions.[20,39−41]

Furthermore, by providing information on the behavior of molecular bonds under the action of a force, this methodology can be very useful also to understand mechanisms of complexes naturally submitted to forces, as those formed between some membrane receptors and their ligands.[42] All of these trademarks make AFS ideal to deeply characterize molecular interactions, and it is becoming more and more frequently used to complement traditional biomolecular approaches.

Pioneer studies have been performed, especially on more stable interactions such as biotin−avidin,[10−13,20,40,43,44] antigens−antibodies,[17,18,45,46] or receptors−ligands.[47,48] Afterward, also many other kinds of biological complexes, different for stability and composition, such as DNA−proteins,[49−51] transient complexes,[29,30] chaperonins with their substrates,[52] or the exotic p53−azurin,[19] have been successfully explored by this technique. Some recent works show the possibility of investigating the interaction between ligands and membrane receptors, probing directly the whole living cells.[53−55] This approach, allowing for mapping of the presence and location of specific receptors on the membrane, provides details about the cellular functional state.

To study a molecular dissociation by AFS, one of the partners has to be bound to a surface and the other one to the AFM tip. The iterating of up and down tip cycles, performed in a physiological buffer, allows for recording dissociation events from which the most probable unbinding force for the complex can be determined. Then, to extract equilibrium information, these data are analyzed in the framework of proper theoretical models.[21,22,26,28,56]

The approach, commonly used to describe the behavior of force-induced transformations, is based on the seminal works of Bell[22] and Evans and Ritchie.[21] Bell's model, proposed for the analysis of bonds responsible for cell to cell adhesion, provides a phenomenological description of the effect of mechanical forces acting on molecular interactions. The main idea of this approach is that a forced dissociation can be considered as a thermally activated escape over a transition-state barrier and treated within the framework of the reaction rate theory. At equilibrium, a receptor−ligand pair changes from the bound (RL) to the unbound (R + L) state, proceeding over a single transition state (R:L) with a characteristic activation free energy barrier ($\Delta G^{\#}$) (Figure 1). The application of an external force alters the energy profile of the unbinding process by lowering the energy of the transition state, thus facilitating

the thermally activated unbinding process. The complex then proceeds via a path characterized by an activation energy barrier reduced by $F \cdot x_\beta$

$$\Delta G(F)^{\#} = \Delta G^{\#} - F \cdot x_\beta \tag{6}$$

where F is the applied force and x_β the width of the energy barrier (see Figure 1). From eq 5, the dissociation rate constant depends on the applied force through

$$k_{off}(F) = k_{off} \cdot \exp(F \cdot x_\beta / k_B T) \tag{7}$$

where k_{off} is the dissociation rate at the equilibrium, with $k_{off} = k_{off}(0)$.

In this framework, Evans and Ritchie described the unbinding process in terms of a crossing over a single, sharp barrier through the application of a time-dependent force $F(t)$.[21,22] Accordingly, the model provides the unbinding force dependence on the loading rate, $R = dF/dt$, at which the external force is applied. R is nominally given by the product, $R = k\upsilon$, between the tip retraction speed (υ) and the spring constant of the cantilever (k). However, in order to avoid introduction of systematic errors, the effective loading rate value should be considered (for more details, see below). The Bell−Evans model is based on the following assumptions: (i) the loading rate during a measurement is constant; (ii) the unbinding process of a single ligand−receptor pair occurs; (iii) the rupture time is longer than the diffusional relaxation time, and any rebinding process is neglected; (iv) the pulling coordinate coincides with the reaction coordinate; and (v) the width of the energy barrier x_β is independent of the applied force. On such a basis, and in the framework of the reaction rate theory, the following probability distribution $P(F)$ of the unbinding force F has been worked out

$$P(F) = \frac{k_{off}}{R} \exp\left[\frac{F x_\beta}{k_B T} + \frac{k_{off} k_B T}{x_\beta R}\left(1 - \exp\left(\frac{F x_\beta}{k_B T}\right)\right)\right] \tag{8}$$

This distribution results in being asymmetric and skewed toward low force values.[57] The most probable unbinding force, F^*, can be then obtained by calculating the maximum of such a distribution, and it is given by

$$F^* = \frac{k_B T}{x_\beta} \ln\left(\frac{R x_\beta}{k_{off} k_B T}\right) \tag{9}$$

This expression predicts a linear relationship between the most probable force, F^*, and the natural logarithm of the loading rate R. By plotting F^* as a function of ln R, the equilibrium parameters k_{off} and x_β can be extracted as the slope and the intercept of a linear fit, respectively. In some cases, the most probable unbinding force as a function of the logarithm of the loading rate exhibits two distinct linear regimes, and then, two sets of k_{off} and x_β values can be extracted by two independent linear fits. Such a behavior may be traced back to the presence of two intermediate states in the unbinding process, instead of a single one.[40,43,44,58] It has been shown that the presence of distinct linear trends for F^* versus ln R could be instead ascribed to a noise-induced effect.[93]

The Bell−Evans model has allowed one to successfully describe the trend of the most probable unbinding force with the loading rate for several ligand−receptor pairs,[18,19,23,34,43,47,59] representing a landmark for describing unbinding processes as studied by AFS, or by other single-molecule techniques, such as biomembrane force probe.[20,21,33] The extracted k_{off} values have been found over a wide range (from 10^{-6} to 150 s^{-1}) for the various biological complexes, indicating a large variability of the kinetic properties of these systems at the single-molecule level. However, the Bell−Evans model, which is still widely used, has revealed some inconsistences. For example, significant discrepancies in the k_{off} values have been obtained from independent measurements on the same systems. Additionally, the unbinding force distributions commonly deviate from that predicted by eq 8, exhibiting asymmetric shape skewed toward high force values.[57,60,61] Furthermore, a nonlinear trend of F^* versus ln R has been observed in some experiments.[26,40]

These observations have led to revision of such a model. The assumption of constant loading rate during the measurements can be questioned, especially at fast loading rates or when flexible linkers are used to connect biomolecules to the solid surfaces.[44,47,58,62] The observed deviations of the unbinding force distribution from that predicted by the Bell−Evans model have been attributed to the heterogeneity in chemical bonds or in the spacer lengths (see the next section).[57,60,61] The Bell−Evans model has been extended to include multiple unbinding processes in which n, equal or different, bonds break.[18,63] The related data have been carefully analyzed by taking into account that the external force can be fully applied or shared among biomolecules, depending on how these are arranged in the experimental setup (e.g., connected serially, in parallel, or in a zipper sequence).[18,64,93] Additionally, the possibility of rebinding should be taken into account, especially for measurements performed in the slow regime.[65] Finally, the assumption that the pulling coordinate coincides with the reaction coordinate has been questioned, and the possible implications for data analysis have been discussed.[66]

Beyond the Bell−Evans approach, more general models of unbinding processes have been developed in the framework of the Kramers theory of thermally activated barriers by introducing an analytical expression for the energy barrier in the presence of an applied force.[26,28] In these models, however, the molecular coordinate has been assumed to fluctuate under the influence of the external force; therefore, the width of the energy barrier, x_β, can no longer be considered as being force-independent. Hummer and Szabo have proposed a model for which the most probable unbinding force depends on the loading rate through $F^* \sim (\ln R)^{1/2}$, while Dudko et al. have derived a model for which $F^* \sim (\ln R)^{2/3}$.[26,28] Remarkably, the trend of the most probable unbinding force with the logarithm of the loading rate, as predicted by these models, including the Bell−Evans one, can be cast into the expression $F^* \sim (\ln R)^{\nu}$, where ν can assume the value 1, 1/2, or 2/3 depending on which model better describes the behavior of the system.[27]

Strategies to Immobilize Proteins on Tips and Supports

The immobilization of proteins on surfaces (tip and substrate) is a crucial aspect of AFS experiments. The anchorage on solid materials has to satisfy some requirements to match the quality of single-molecule recognition studies. The protein native structure is to be preserved upon immobilization. The proteins should maintain a sufficient mobility and reorientational freedom in order to favor the exposure of the binding site and, consequently, the interaction with the partner. The immobilization procedure has also to ensure that, when the tip moves back, the proteins do not detach from the tip and support, but only the

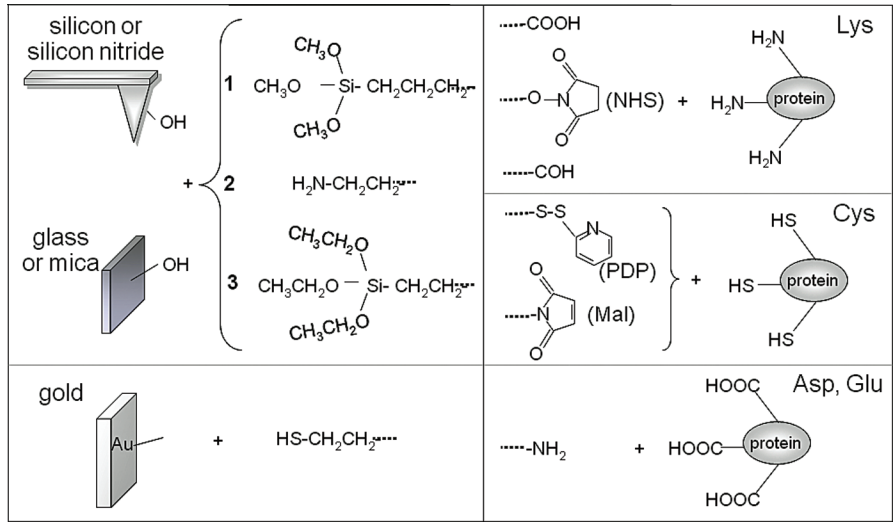

Figure 2. Reactions commonly used to immobilize proteins to different surfaces by linking various amino acids. (NHS = *N*-hydroxysuccinimide; PDP = pyridyldithiopropionate; Mal = maleimide; Lys = lysine; Cys = cysteine; Asp = aspartic acid; Glu = glutamic acid).

protein−protein bond breaks, enabling also cyclic registration of the force curves. To this aim, immobilization on the surfaces by means of covalent bonds is usually preferred, provided that the interacting regions of the biomolecules remain available for the biorecognition process. Finally, the immobilization strategies should maximize the probability that a single ligand−receptor pair may be involved by also minimizing the occurrence of nonspecific interactions.

The chemistry used to anchor molecules, the coverage, and the protein functionality depend on the properties of tip and support surfaces. The tip and support are available of different materials. Tips are usually made of silicon or silicon nitride. If conveniently treated with chemical or physical procedures, they provide hydroxyl groups that can react with specific groups of molecules to form covalent bonds (Figure 2). Sometimes, tips can be coated with gold, and in this case the strong affinity of this material for sulphidryl groups may be exploited to covalently immobilize the biomolecules.[67]

The most frequently used supports are silicon wafers, glass slides, and mica. They all can expose hydroxyls, so that the same chemistry developed for silicon tips can be used. Additionally, surfaces can anchor proteins through electrostatic interactions.[1,23] Gold slides are sometimes used to immobilize proteins, again by exploiting the affinity of sulphidryl groups for gold. We note on passing that gold provides the opportunity of coupling conductive techniques to AFS, allowing one to gain complementary information from a multisensing approach. Given its conductive properties, gold can be used as an electrode to study possible electron-transfer properties of proteins.[67] Finally, gold substrates offer the possibility to study dissociation kinetics of biological molecules by both AFS and surface plasmon resonance. In this way, a direct comparison of the interaction properties of the molecules, with and without an applied force, can be performed.[68]

The first studies performed by AFS were oriented to investigate the strength of the interaction between biotin and avidin.[10−12] In that time, it was quite common to anchor the proteins directly on silicon nitride tips and mica or glass supports.[10−12,69] As long as AFS has been applied to investigate other complexes, the immobilization procedures have become more refined. Today, almost all of the immobilizations are achieved by means of linkers which carry two different functional ends, one for anchoring to the inorganic surface and the other to target specific functional groups of the biomolecule or of another linker.[23] In general, the methodologies to anchor proteins by means of linkers can be divided into two major classes, those exploiting flexible linkers[17−20,30,45,70,71] and those exploiting more rigid spacers;[46,52,72−74] a combination of both can also be found.[17,58,75−77] A preliminary functionalization of the surfaces with self-assembled short spacers with one end suitable for reaction with the surfaces and the other for reacting with other molecules (linkers or biomolecules) has been often used. For example, gold or gold-coated surfaces (substrates or tips) can be functionalized with alkanthiols, such as cysteamine.[30] Glass substrates, silicon, or silicon nitride tips can be functionalized with silanes or alcohol-based spacers, such as ethanolamine, after a chemical or physical treatment to expose hydroxyl groups.[23,47,58] On the left side of Figure 2, some representative examples of functional groups exposed by linkers frequently used to covalently bind solid supports are shown. On the right side of this figure, we can see how amino acidic residues of proteins can form covalent bonds with the remaining spacer free ends. For example, aminic groups are available from lysines, which are amino acids rather commonly found in the proteins. At variance, cysteines, which expose sulphidryl groups, are amino acids not always found in the proteins. For this reason, when available, their binding results in a specific orientation of the biomolecule. Also, carboxyl groups, available on aspartic and glutamic acids, are sometimes used to covalently link proteins, although they have to be previously activated.

One of the mostly used flexible linker in AFS experiments is the heterobifunctional polyethylene glycol (PEG), a versatile polymer with well-characterized stretching properties which can be synthesized at different lengths and with different functionalized ends.[45,76]

The above description of immobilization strategies is not exhaustive since more refined and specific procedures are continuously proposed in the literature. For example, it has been suggested that single-walled carbon nanotubes can be used as small probes to measure unbinding forces of single protein−protein interactions, with the possibility of mapping recognition partners with true molecular resolution.[78] Moreover, engineered proteins, bearing a His tag or a glutathione S-transferase (GST) tail, can be specifically immobilized by exploiting their affinity for nickel ions and for glutathione, respectively, even if these strategies are not appropriate in many cases due to a weak binding to the surface.[25,79]

Generally, the use of linkers, placing proteins away from the rigid surfaces, prevents possible distortion of protein structures, arising from their direct interaction with the inorganic materials. Moreover, linkers allow the proteins to retain some reorientional freedom in the environment, favoring the biorecognition process. On the other hand, the introduction of long elastic tethers between proteins and supports locates the specific unbinding events far away from the sample surface, while the nonspecific ones remain near the tip−support interface, making their discrimination easier (see also below).[18,25,29,49,76]

As stated above, an ideal AFS unbinding experiment should involve possibly a single ligand−receptor pair. Such a goal could be better reached if the substrate and tip were bonded with the biomolecules at a low coverage. However, several AFS experiments are performed with a full coverage of receptor molecules on the substrate and a low density of ligands on the tip. These conditions, besides favoring multiple events, can also give rise to some steric hindrance, with some hampering of the binding process. To achieve a controlled density of biomolecules on the surfaces, functionalization strategies using a mixing of linkers with different capabilities to target biomolecules have been developed.[80] For example, linkers bearing on one end a protein-resistant group (e.g., oligoethylene glycol (OEG)) can be mixed with linkers able to target specific protein functional groups.[81] By varying the ratio between active and inactive spacers, a modulation of the density of the proteins on the substrate can be obtained even if the possibility to still have a high local density cannot be ruled out.[18,23,76,82,83] To visualize isolated biomolecules by AFM imaging, the use of substrates with a low roughness, such as bare mica or annealed gold substrates, is preferred. The height of the AFM imaged spot can be then compared with the expected dimensions of the biomolecules in order to ascertain if some denaturation has taken place.[84] When substrates with high molecular coverage are used, the thickness of the molecular film can be evaluated by performing scratching by AFM in contact mode and compared with that expected from a single biomolecular layer.[19,83] On the other hand, a reliable check of the molecular density on the tip is difficult to obtain. However, specific protocols to reduce such a density have been provided.[23]

When the regions at which two proteins interact are not known, it can be useful to investigate their binding by docking studies, aiming at predicting the most probable complex configuration. Docking is a computational approach that, starting from the independently determined three-dimensional structures of molecules, probes their full surfaces, looking for all of the possible binding modes. The resulting configurations are ranked based on a scoring function, taking into consideration different interface parameters, depending on the docking method used.[85] Further refining leads to modeling of the most probable three-dimensional structure for the complex, providing useful information to select a proper immobilization procedure for the biomolecules leaving the interaction regions available for biorecognition.[86,87]

Force−Distance Curves and Data Analysis

To record the force−distance curves in AFS experiments, the ligand-functionalized tip and receptor-functionalized support are approached and retracted; such a process can be also done in a cyclic way. The outcome of this process is a force curve, formed by a trace and a retrace line, like that shown in Figure 3a, in which the tip displacement is plotted versus the deflection of the cantilever. At point 1, the tip is far from the support, and thus, the cantilever deflection is zero. Then, the tip goes down,

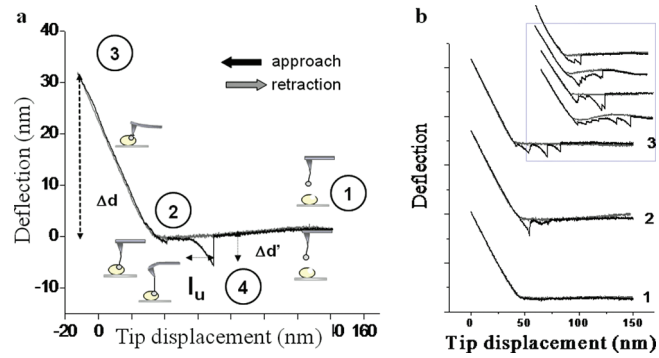

Figure 3. (a) Typical approach and retraction force−distance curve displaying a specific unbinding event between two biomolecular partners. (b) Representative real force−distance curves commonly detected in AFS experiments (see the text). Inset: examples of ambiguous force−distance curves.

approaching the support at point 2, and the cantilever deflection changes. During such a step, if the two partners are endowed with enough flexibility and reorientational freedom to assume a correct reciprocal orientation, they may undergo a biorecognition process, forming a specific complex. Further pushing of the tip makes the deflection increase, reaching a maximum preset value at point 3. The deflection, Δd, at this point, multiplied by the spring constant gives the force applied by the tip on the support, with such a value being usually kept below 1 nN in order to avoid protein damage. The tip is then retracted, and adhesion forces and/or interaction bonds formed in the contact phase between molecules cause the tip to adhere to the sample up to some distance beyond the initial contact point. As far as the retraction continues, the spring force overcomes the interaction forces, and the cantilever jumps off, sharply returning to the zero deflection level at point 4 (jump-off contact). Such a jump is characterized by the deflection $\Delta d'$, which can be converted into a force by multiplying it by the cantilever spring constant. If a specific complex between the ligand and the receptor has been formed during the approach, $\Delta d'$ can give an estimation of the rupture or unbinding force of the complex. Notably, the effective value of the cantilever spring constant has to be experimentally measured after the acquirement of data. There are various methods by which this can be done, mainly based on the thermal noise analysis[88] or on the measurement of the resonant frequency.[89] Finally, the cantilever is retracted to the initial position until point 1.

In AFS experiments, a large number of curves, hundreds or even thousands, are commonly registered. These curves are acquired at the same location or even at different regions of the substrate. In both cases, the presence of a slight drift in the $x-y$ plane should be considered when long time experiments are performed.

Besides the curve shown in Figure 3a, other representative curves obtainable from AFS experiments are shown in Figure 3b.[25,90,91] In curve 1, the retrace faithfully follows the approach line, meaning that no events have been recorded.[25,47] Curve 2 retains the same linear slope of the contact region during the retraction, before the jump-off event; such a behavior is usually attributed to a tip−support interaction without the involvement of specific binding between the proteins.[19,25,90,91] Both curve 1 and curve 2 are discarded. Curve 3 shows multiple jumps which can arise from a variety of phenomena, such as a partial stretching of molecules (similar to that observed during unfolding AFS experiments[15]), nonspecific interactions, contact between molecules immobilized away from the tip apex, and so forth. When multiple events occur, researchers are often led to

consider only the last jump-off, if it starts and ends at zero deflection, as that of Figure 3a.[71,92]

Finally, in the inset of Figure 3b, we have collected other examples of curves that are characterized by ambiguous shapes from which it is difficult to select specific events. For this reason, they are often discarded to avoid the introduction of spurious values in the data collection.

In addition to the above-mentioned criteria, other ones are currently adopted to distinguish specific from nonspecific events. For example, when both of the partners are immobilized by flexible linkers, it is reasonable to expect that the complex dissociation will occur after the polymers have been almost completely stretched (about 90%), the related curves exhibiting a change in the slope during the retraction process. More specifically, curves showing a jump-off event occurring at an unbinding length, l_u, (see Figure 3a), corresponding to the estimated linker stretching, are commonly accepted.[18,64,93,94] In this respect, the force versus extension characteristics can be predicted in terms of models, such as the worm-like chain[95,96] and the freely joined chain.[97] Furthermore, the use of long tethers, giving rise to a more marked stretching, should be preferred.[76,96]

If, on one hand, elastic linkers can help to select specific unbinding events, on the other, they can introduce some complications into the data analysis, as recently emphasized. In particular, the stretching of linkers could affect the real loading rate values.[62] An estimation of the effective loading rate ($R = k_{sys}v$) should take into account the effective spring constant of the system, k_{sys}, which can be measured from the slope of the retraction curve; such a procedure would avoid the introduction of systematic errors in the extraction of k_{off}. Furthermore, since flexible polymer linkers may undergo a stretching process resulting in a variable path from curve to curve, also depending on the applied force, the assumption of a constant loading rate may no longer be valid. In this respect, procedures to extract the most probable value of the loading rate by a statistical analysis of a series of curves or by introduction analytical accurate models of the stretching have been proposed.[62,93,98,99]

The unbinding frequency can be evaluated by the ratio between events corresponding to specific unbinding processes and the total recorded events. Unbinding frequencies ranging from 10 to even 85% have been registered for different ligand−receptor pairs.[17,29,44,72,97] Lower unbinding frequencies could be due to a variety of reasons, such as the randomized orientation of molecules, a low molecular density, molecular clustering, partial denaturation of the molecules, and so forth.

Further assessment of the specificity of the recorded events can be obtained by some control experiments. For example, experiments in which the biorecognition process between the biomolecules is inhibited (blocking) through the addition of the corresponding free partner to the substrate or to the tip can be performed.[11,17,25,29,45,97,100] Alternatively, experiments can be repeated without attaching any biomolecule to the linkers or by modifying the setup by adding or removing molecular species which regulate the partners' binding, such as Ca^+, or by changing the pH of the solution.[101] Together with a decrease of specific interaction, blocking could also reduce nonspecific interactions. In this respect, to further verify the specificity of the interaction, AFS experiments should be performed also by substituting one of the partners with a molecule which is known to not interact with the other biomolecule.[25]

The unbinding force values obtained from a collection of curves assigned to specific events are used to generate histograms, with a binning h normally kept higher than 5 pN. The optimal bin size can be estimated by minimizing the integral of the mean-square errors, and it is approximated by $h = 3.5\sigma n^{-1/2}$, where σ is the standard deviation of the distribution and n is the total number of data points.[101] As stated above, most of the experimental distributions are quite spread and generally asymmetric with a skew toward higher force values, at variance with what is predicted by eq 8.[18,57,60,61] Additionally, multiple peaks are often observed.[11,19] This variability could be ascribed to several factors, such as heterogeneity in the formation of ligand−receptor pairs, slight differences in the relative arrangements of the partners, the existence of different binding sites, the occurrence of multiple unbinding processes, the stretching of molecules, and so forth.[18] Theoretical models to quantitatively describe these effects have been proposed.[57,60] Once the unbinding force histograms have been built, the problem to be faced is the determination of the most probable unbinding force in order to apply the Bell−Evans model (eq 9).

For a single peak distribution, the most probable unbinding force can be evaluated from the maximum of the distribution, which is extracted by a Gaussian fit.[19,60] In this respect, it should be remarked that systematic errors could be introduced since contributions from high force values are neglected. The presence of clearly distinguishable peaks in the histograms have been put into a relationship to the occurrence of multiple unbinding events occurring in parallel.[12] When these peaks are equally spaced, the distance between two subsequent peaks has been assumed as the quantum for the unbinding force.[12,19,44,73] However, the occurrence of multiple unbinding events does not necessarily give rise to multiple peaks in the histograms.[18,55,71,102] For example, when n biomolecular partners are pulled at the same time, the effectively applied loading rate can be shared among them, that is, the real loading rate can be $1/n$, the global value,[10,18] and the corresponding unbinding force distributions may then display no quantization. On the other hand, when the unbinding of different pairs takes place in sequence, the whole force is applied to each pair. In this respect, more accurate procedures to analyze force distributions in the presence of multiple unbinding events have been developed.[10,18,93] Most currently, the analysis is restricted to the first or to the second peak of the distribution, from which the most probable unbinding force is evaluated.[18,19,29] Nevertheless, it is important to reduce as much as possible the occurrence of multiple dissociations. Samples at low coverage certainly can be useful to this purpose, favoring the resolution of the single bond rupture, together with the adoption of strategies which help in discriminating between single and multiple bonds.

Finally, long and tedious analysis of the force curves may take advantage of automated procedures to detect and process the data, as recently developed.[71,102]

Azurin−Cytochrome c551 Interaction by AFS: Strategies and Results

We have investigated by AFS the complex formed by azurin and cytochrome c551, two proteins from the bacterium *Pseudomonas aeruginosa*. The interaction between azurin and cytochrome c551 has a transient character, allowing the electron transfer to take place with optimal efficiency.[103] Redox metalloproteins have gained particular interest because of the challenge of integrating them with electronic transducers in order to implement hybrid nanodevices for biosensing applications.[104]

Since the structure of the complex between the proteins was not available, we have preliminarily performed a computational docking study by using the GRAMM algorithm, which searches for the best steric fit between molecules by taking into account hydrophobic interactions.[105] The best complex that emerged

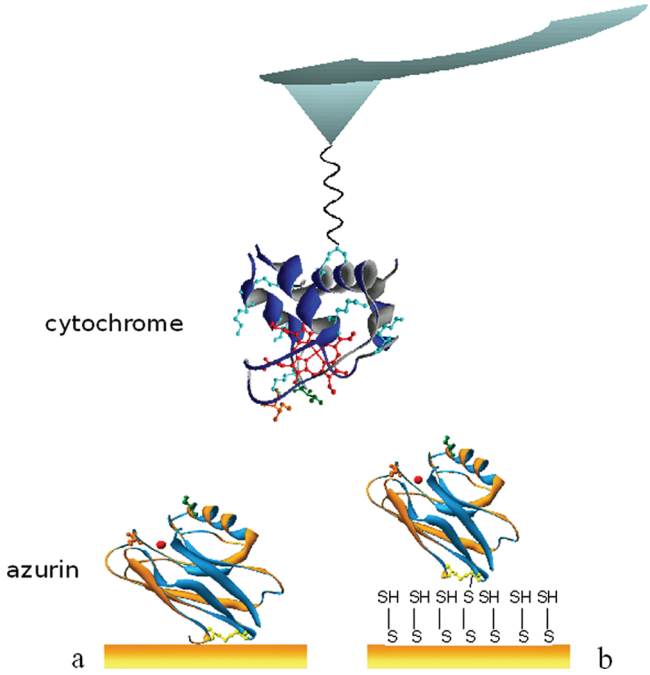

Figure 4. Schematic illustration of the immobilization strategy used for studying the unbinding process of the azurin−cytochrome c551 complex. Cytochrome c551 is linked to the tip by a PEG spacer binding its lysine residues. Azurin is immobilized on gold substrate by its native disulfide group (a) through direct linking or (b) by means of a spacer.

from this docking approach is characterized by a close contact between the hydrophobic regions of the two proteins, with azurin possessing a single disulfide bridge which is at the opposite side with respect to the binding region.[106] On the basis of these results, we have developed two different immobilization strategies to favor, at best, a correct interaction between the partners in the AFS study (see Figure 4).

At first, cytochrome c551 was immobilized onto the tip by using a 10 nm long PEG spacer.[29] On one end, the spacer was linked to the tip by an aldehyde moiety, and on the other, it was bound to cytochrome through a carboxyl group. Such a functional group is able to target one of the eight available lysine residues homogeneously distributed on the protein surface, and this leads, very likely, to a random orientation of the protein molecules on the tip (for more details, see refs 29 and 30). Azurin has been deposited directly on bare gold by exploiting the high affinity for gold of its disulfide bridge (Figure 4a).[24] Accordingly, all of the azurin molecules are expected to be uniformly oriented with their binding site facing the C551 partner. The azurin molecules resulted in being self-assembled on the gold substrate as a dense protein monolayer whose topological features have been checked by AFM imaging. An almost full coverage with a mean height of (1.7 ± 0.6) nm over the gold surface has been observed; such a value is lower than that expected from the X-ray structure. This might arise either from a deformation of the proteins arising from compression exerted by the AFM tip or from a partial denaturation of the azurin molecules which are in direct contact with the gold surface (see refs 29 and 30).

Several force curves, recorded at different loading rates, have been analyzed by taking into account the procedures and the criteria previously described. In particular, we verified that the selected curves displayed, before the jump-off, a delayed nonlinear course (Figure 3a) with the stretching features of used PEG.[25]

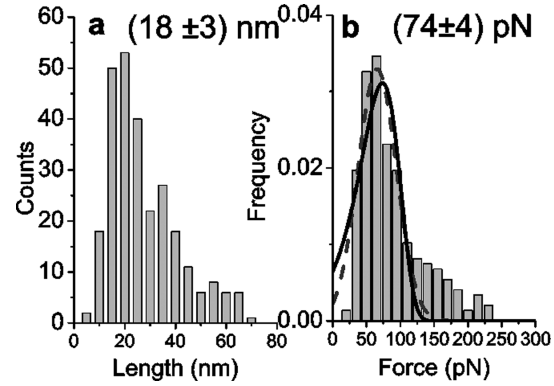

Figure 5. (a) Unbinding length and (b) unbinding force distributions for the azurin−cytochrome c551 complex immobilized through the strategy shown in Figure 4a; the force curves have been recorded at the nominal loading rate of 5 nN/s. Dashed line: the fitted Gaussian distribution to extract the most probable unbinding force value. Continuous line: the Bell−Evans distribution as obtained from eq 8 by inserting the values for the effective loading rate, the dissociation rate ($k_{off} = 14\ s^{-1}$), and the energy barrier width ($x_\beta = 0.14$ nm). The extracted central values of the fitted Gaussian distributions and the related statistical errors, obtained by $2\sigma/N^{1/2}$ for a 95.4% confidence level, are reported.

The distributions of the unbinding lengths and forces obtained at the nominal loading rate of 5 nN/s are shown in Figure 5a and b, respectively. The unbinding length distribution is characterized by a main mode centered at around 18 nm. This value is in a good agreement with those found in other AFS experiments using PEG linkers of the same length (10 nm)[45,95] and is consistent with the expected length of the PEG under stretching, this being estimated as approximately twice the unstretched value by applying the freely jointed chain model.[97] This result strongly indicates that the observed jump-offs are due to a dissociation of the complex occurring after the linker has been stretched. The histogram of the unbinding forces exhibits a single mode with an asymmetric shape and a skew toward high force values. This shape is at variance with that expected from the Bell−Evans model, given in eq 8, but is quite similar to what is commonly observed in other systems (see also below).[18,59,76,99] This discrepancy could be attributed to several factors, such as multiple binding events, binding heterogeneity, and so forth, as recalled in the previous section. The most probable unbinding force, evaluated from the maximum of the distribution, has been found to be around 74 pN by a Gaussian fit (see the dashed line in Figure 5b). As already mentioned, the Gaussian fit of the distribution describes the unbinding force around the main peak, neglecting the higher force values.

An unbinding frequency percentage of 18% has been found. Such a rather low value is consistent with the random distribution of the anchoring sites and hence of the interacting sites. However, it is close to the values recorded in other systems.[59,73]

To confirm the specificity of detected events, we have performed a control experiment, in which free azurin was added to the fluid cell in order to contain the cytochrome-functionalized substrate. In these conditions, the unbinding frequency is reduced from the initial average value of 18 down to 5.5%, therefore resulting in a 70% decrease of unbinding events. The unbinding force distributions, before and during tip blocking, have been analyzed and compared, as shown in Figure 6. Besides the reduction of unbinding events, it can be noted that the force distribution shape is rather similar to that occurring before blocking. This seems to indicate that the largest part of the survived events has the same features as the initial ones, consistent with a residual specific activity between azurin and

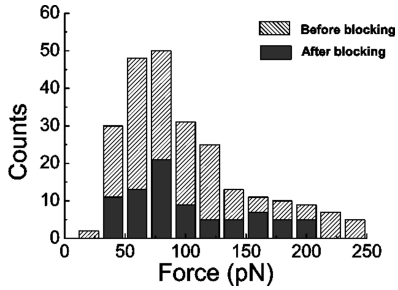

Figure 6. Unbinding force distributions for the azurin−cytochrome c551 complex immobilized through the strategy shown in Figure 4a, before (gray) and after (black) blocking. The force curves have been recorded at the nominal loading rate of 5 nN/s.

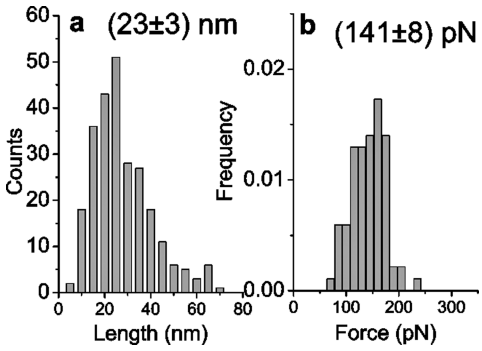

Figure 7. (a) Unbinding length and (b) unbinding force distributions for the azurin−cytochrome c551 complex, immobilized through the strategy shown in Figure 4b. The force curves have been recorded at the nominal loading rate of 5 nN/s. The extracted central values of the fitted Gaussian distributions and the related statistical errors, obtained by $2\sigma/N^{1/2}$ for a 95.4% confidence level, are reported.

cytochrome after the blocking. However, a concomitant reduction of nonspecific interactions cannot be ruled out.

In the second approach, azurin has been immobilized onto gold via a cysteamine-*N*-succinimidyl-3-(*S*-acetylthio)propionate (SATP) spacer that binds the thiol group of the protein (Figure 4b). The tip was functionalized with the same procedure as that followed in the first approach. From AFM imaging of the substrate, we have assessed the presence of a submonolayer coverage, with a mean spot height of (3.4 ± 0.8) nm. Such a value matches the expected height from crystallographic data of azurin well,[107] indicating that this second immobilization architecture better preserves the protein native structure.

Again, we have recorded force curves at different loading rates; the corresponding unbinding length and force distributions, at the nominal loading rate of 5 nN/s, are shown in Figure 7. The unbinding length distribution exhibits a single-mode distribution centered at 23 ± 4 nm; such a value is in a satisfactory agreement with that obtained by the first approach (see Figure 5) and is consistent with the involvement of the linker in the unbinding process. However, the observed unbinding length, slightly exceeding the expected value (about 20 nm), could be due to the stretching of the linkers used to immobilize azurin or even to a partial stretching of the involved biomolecules. The histogram of the unbinding forces is characterized by a single peak. Remarkably, this distribution exhibits an asymmetric shape with some skew toward low force values, in agreement with what expected is from the Bell−Evans model.[57] The extracted most probable unbinding force value is 141 pN; such a value is shifted to a significantly higher value with respect to that observed in the previous experiments (74 pN) at the same loading rate. A similar shift has been also obtained for the other

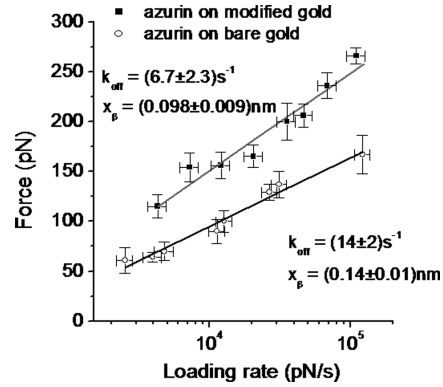

Figure 8. The most probable unbinding force dependence on the logarithm of the loading rate for the azurin−cytochrome c551 complex when azurin is immobilized on bare gold (open circles) and on modified gold (squares). Errors in the unbinding force have been derived from the standard deviation of the related distribution. Errors in the loading rate, $R = k_{sys}v$, have been evaluated by the error propagation, where the error of k_{sys} has been estimated as the uncertainty in the slope of the retraction curve while the errors on v have been derived from the experimental apparatus. The solid lines are numerical fits of the experimental data to the Bell−Evans model (eq 9); the extracted values for the parameters k_{off} and x_β have been reported.

loading rate values. This indicates that the immobilization strategy can sometimes modify the interaction forces.

An unbinding frequency of about 9% has been observed; such a value was decreased in comparison to that registered in the previous experiment, likely due to a lowered interacting probability arising from the reduced protein density on the support. Control blocking experiments have confirmed the specificity of the observed events, resulting in a 63% reduction of the unbinding frequency.

For both of the immobilization procedures, the most probable unbinding forces have been plotted as a function of the logarithm of the effective loading rate, as evaluated from the slope of the retraction curve.

A linear trend has been observed for both cases over almost 2 orders of magnitude of loading rate (see Figure 8). In the framework of the Bell−Evans model, it comes out that a single regime corresponding to a unique energy barrier characterizes the process from the bound to the unbound state. By fitting these data by eq 9, we have obtained a dissociation rate k_{off} of about 14 s^{-1} and a width of the energy barrier around 0.14 nm for azurin directly chemisorbed on gold. By inserting these values together with the effective loading rate, in eq 8, the expected Bell−Evans distribution for the unbinding force can be derived. This theoretical distribution, also shown in Figure 5b (continuous line), describes rather well the experimental points around the most probable value, where it almost overlaps the Gaussian distribution (dashed line).

On the other hand, for azurin immobilized on gold via the linker, a dissociation rate k_{off} of about 7 s^{-1} and a width of the energy barrier around 0.1 nm have been extracted. The rather high dissociation rate is indicative of a quite fast dissociation, consistent with the transient nature of the complex under investigation.[108] The lower dissociation rate value found in the case of azurin on modified gold with respect to azurin directly immobilized on gold suggests that azurin fits more tightly to cytochrome when the linkage to the conductive substrate is accomplished via a spacer. Since smaller potential barrier widths reflect a protein resistance against bond rupture,[53] the found values are indicative of a more specific recognition occurring when azurin is immobilized through a linker. Such a result finds

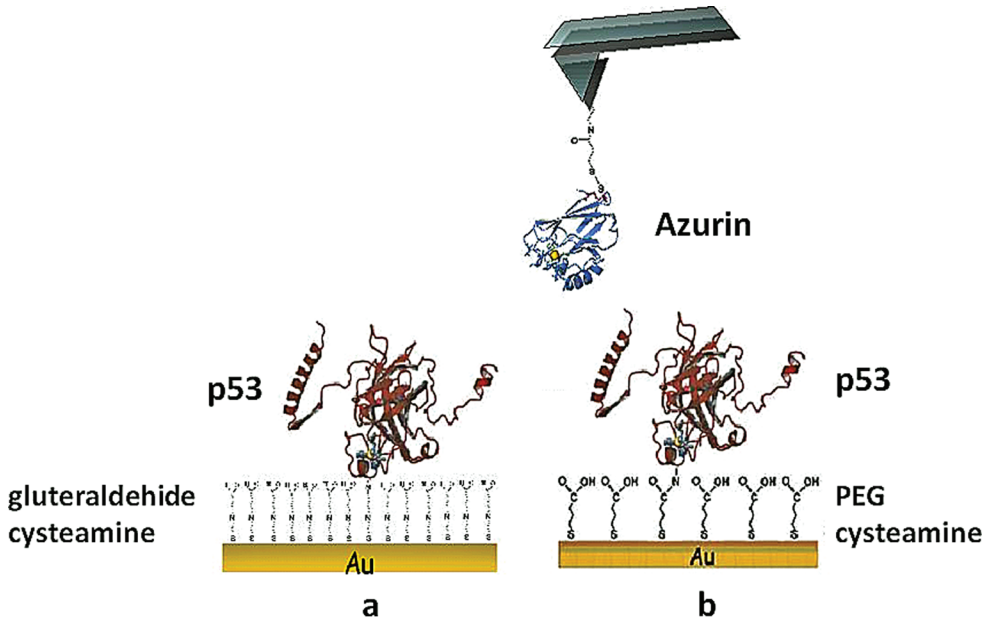

Figure 9. Schematic illustration of the immobilization strategy used for studying the unbinding process of the p53−azurin complex. Azurin is covalently linked to the tip via the sulfhydryl-terminated spacer (SATP) that can bind one of the two accessible cysteine residues of the disulfide group. The p53 is immobilized on gold substrate by one of the exposed lysines of p53 to (a) a glutaraldehide cysteamine or (b) a PEG spacer.

a correspondence with the fact that the use of organic spacers to immobilize the protein better maintains the expected height of proteins and presumably their native state, also conferring a higher reorientational freedom for optimal interaction with its counterpart. Moreover, this study has demonstrated that AFS can be successfully applied to investigate not only very stable complexes but also transient ones, gaining insight into these interesting electron-transfer biomolecular pairs.[24]

Disclosing p53−Azurin Interactions by AFS

Dynamic force spectroscopy has been applied to ascertain the formation of a complex between the human tumor suppressor protein p53 and the bacterial protein azurin, which has been suggested to promote the p53-related cancer defense mechanisms.[109,110]

We have preliminarily performed docking studies to provide a possible configuration for the p53−azurin complex.[86,87] To this aim, we have used the Zdock docking program, which combines pairwise shape complementary with desolvation and electrostatics.[111] This computational investigation has led us to predict two possible best complex configurations for the interaction of azurin with p53, one involving the DNA binding domain of p53 and the other one the N-terminal domain of p53, according to refs 112 and 113. These outcomes have been used for developing two appropriate immobilization strategies to investigate the formation of the p53−azurin complex by AFS (see Figure 9).

In the first strategy, we have linked azurin to the tip by a short sulphidryl-terminated spacer, involving SATP, binding one of its two cysteine residues of the disulfide bridge (see Figure 9a). This procedure is very similar to that previously used to study the interaction of azurin with cytochrome and was found to preserve the protein functionality. According to computational docking results, this link is susceptible to provide a correct orientation of azurin with respect to p53 by leaving the azurin hydrophobic patch available for the interaction with the partner. The p53 has been instead immobilized onto a gold substrate via a cysteamine−glutaraldehyde spacer suitable to bind one of its exposed lysine residues.

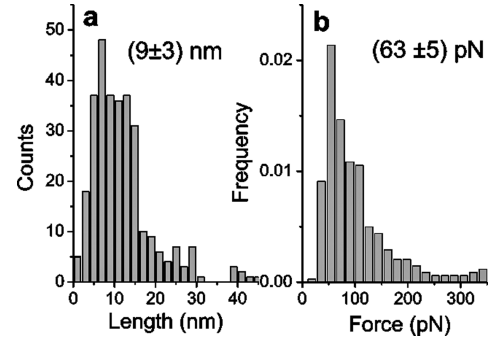

Figure 10. (a) Unbinding length and (b) unbinding force distributions for the p53−azurin complex, immobilized through the strategy shown in Figure 9a. The force curves have been recorded at the nominal loading rate of 4.5 nN/s. The extracted central values of the fitted Gaussian distributions and the related statistical errors, obtained by $2\sigma/N^{1/2}$ for a 95.4% confidence level, are reported.

Analysis of the force curves recorded at different loading rates has been performed by following the same criteria adopted for the azurin−cytochrome complex. The distributions of the unbinding lengths and unbinding forces, obtained at the nominal loading rate of 4.5 nN/s, are shown in Figure 10a and b, respectively. The unbinding length distribution reveals a peak at around 9 nm; such a value is rather low but consistent with the short linkers used for the biomolecule immobilization. The unbinding force distribution is asymmetric, with a main peak skewed toward higher force values, at odds with what is expected from eq 8. The most probable unbinding force extracted from the maximum of the distribution is about 63 pN. An unbinding frequency of about 15% has been found. A reduction of the unbinding frequency of about 42% has been observed by blocking the p53 monolayer with the introduction of a solution of free azurin molecules into the fluid cell containing the p53-functionalized substrate. A comparison of unbinding force distributions of events recorded before and after blocking reveals a rearrangement of the force distribution after blocking (Figure 11). We can identify two regions on the histogram, a first one in which there is the main peak, centered at around 50 pN, and a second one with a peak centered at

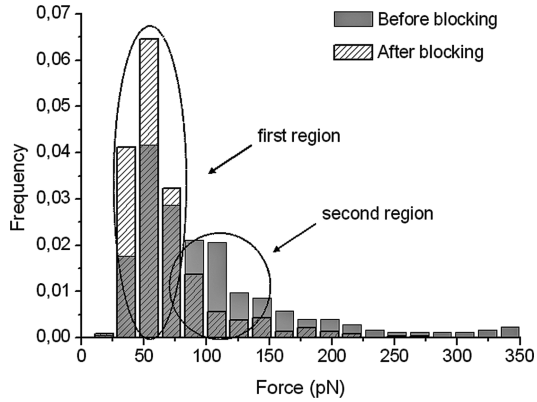

Figure 11. Unbinding force distributions for the p53−azurin interaction, immobilized through the strategy shown in Figure 9a, before (gray) and after (light gray) blocking. The force curves have been recorded at the nominal loading rate 4.5 nN/s.

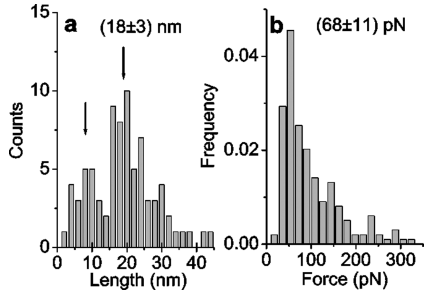

Figure 12. (a) Unbinding length and (b) unbinding force distributions for the p53−azurin complex, immobilized through the strategy shown in Figure 9b. The force curves have been recorded at the nominal loading rate of 4.5 nN/s. The extracted central values of the fitted Gaussian distributions and the related statistical errors, obtained by $2\sigma/N^{1/2}$ for a 95.4% confidence level, are reported.

around 100 pN. Although the total unbinding frequency is lowered after blocking, events falling within the first region of the histogram are increased, whereas those in the second region are reduced. This lead us to hypothesize that events related to the main peak could be due to nonspecific interactions, while specific ones are placed especially in the region at higher forces, at which the occurrence is reduced during blocking. We have then reanalyzed our data by discarding those force curves whose unbinding length is less than 10 nm in order to reduce the contribution from nonspecific events. In this case, we have found that that the most probable force increases up to 74 pN. We then obtained an unbinding frequency of about 12%, and after blocking the p53 monolayer with free azurin molecules, we observed a reduction of the unbinding frequency of 55%.[17,95]

According to the second strategy, p53 has been immobilized on the substrate by substituting glutaraldehyde with a 5 nm PEG linker, as shown in Figure 9b (for more details, see ref 19). Indeed, the cysteamine−glutaraldehyde spacer used in the first approach was probably not able to provide the protein with a sufficient reorientational freedom to favor the binding with azurin (and probably favored the occurrence of nonspecific adhesions).

The distributions of the unbinding lengths and forces, at the nominal loading rate of 4.5 nN/s, are shown in Figure 12a and b, respectively. The unbinding length distribution displays two peaks, one centered at around 8 nm and the other one, more intense, at about 18 nm (see the arrows in Figure 12a). The latter value can reasonably arise from the PEG stretching (about 8−10 nm), from the stretching due to the other linker (cysteamine−glutaraldehyde spacer), and possibly from a partial

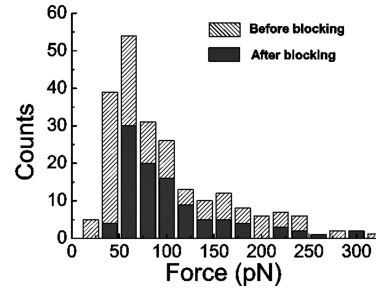

Figure 13. Unbinding force distributions for the p53−azurin interaction, immobilized through the strategy shown in Figure 9b, before (gray) and after (black) blocking. The force curves have been recorded at the nominal loading rate 4.5 nN/s.

stretching of the biomolecules. We can therefore attribute this peak to specific unbinding events for this double tethered configuration. The higher number of specific events found for this peak in the presence of the PEG tether likely derives from a higher reorientational freedom conferred by the tether to p53. Notably, selection of specific from nonspecific events is greatly facilitated when the immobilization of proteins is achieved by longer, flexible linkers.[18,76,99] At variance, for short, rigid linkers, the distance at which nonspecific interactions take place almost overlaps with that of specific events, as observed in Figure 10b.

The unbinding force distribution obtained by considering only force curves with unbinding lengths higher than 10 nm is shown in Figure 12b. The histogram is characterized by a main peak at about 68 nN with some broadening toward higher force values; a fit by Gaussian describes the main peak well (see the dashed line in Figure 12b). The contribution of higher force value to the distribution becomes more marked by increasing the loading rate, suggesting the presence of additional effects, as previously discussed. An unbinding frequency ranging between 15 and 21% has been observed for a collection of experiments performed under the same conditions. The specificity of the observed interactions has been checked by repeating the AFS experiments after blocking the p53 monolayer by a free azurin solution. These conditions have led to a reduction of the unbinding frequency of about 63%. By comparing the unbinding force distributions obtained before and after blocking (Figure 13), we note a lowering of the number of events over the whole histogram, unlike what was observed in the previous experiment (Figure 10). The similarity of the two distributions in Figure 13 suggests that events recorded before blocking are due to specific interactions between the proteins. All of these results support the formation of a specific complex between p53 and azurin, this being particularly relevant in connection with a possible anticancer role of azurin through a stabilization of p53.

Kinetics information on this complex has been gained by analyzing the dependence of the most probable unbinding force on the applied loading rate for the two developed immobilization strategies. In both cases, a linear trend of the force with the logarithm of the loading rate has been registered, (Figure 14). This indicates that the Bell−Evans model can provide a good description of the unbinding process in terms of a single barrier separating the bound from the unbound state of these two proteins. By fitting the data by eq 9, we have estimated the dissociation rate k_{off} and the width of the energy barrier x_β. For the first immobilization strategy, we have found a k_{off} of about 0.14 s^{-1} and a x_β of about 0.46 nm. We note that significantly different values have been obtained for both k_{off} and x_β when all of the unbinding curves are used in the analysis (0.32 s^{-1} for k_{off} and 0.34 nm for x_β). This confirms that the selection of curves is a crucial point of the data analysis procedure. For the

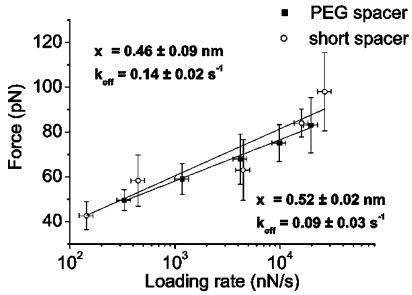

Figure 14. The most probable unbinding force dependence on the logarithm of the loading rate for the p53−azurin complex, when p53 is immobilized via cysteamine−glutaraldehyde (open circles) and via PEG (squares). Errors on the unbinding force have been derived from the standard deviation of the related distribution. Errors on the loading rate, $R = k_{sys}v$, have been evaluated by the error propagation, where the error of k_{sys} has been estimated as the uncertainty in the slope of the retraction curve while the errors on v have been derived from experimental apparatus.The solid lines are numerical fits of the experimental data to the Bell−Evans model (eq 9); the extracted parameters are reported.

second strategy, we have estimated a dissociation rate k_{off} of 0.09 s^{-1} and a width of the energy barrier x_β of 0.52 nm. We observed that the kinetic properties of the systems may be somewhat affected by the adopted immobilization strategy. All of the considerations made about the selection of specific events and biorecognition efficiency might suggest that the second strategy and therefore corresponding kinetic parameters better describe the interaction process between p53 and azurin. In such a case, we have further analyzed the data by estimating the association rate, k_{on}, for the p53−azurin interaction. By following the procedure reported in ref 45, an estimation of k_{on} can be performed through the expression $k_{on} = N_A V_{eff}/t_{0.5}$, where N_A is Avogadro's number, V_{eff} is the effective volume of a half-sphere with radius r_{eff} around the tip, and $t_{0.5}$ is the time for the half-maximal binding probability, given by $t_{0.5} = 2r_{eff}/v$, where v is the approach speed of the cantilever. To estimate $t_{0.5}$, we have varied the interaction time between the proteins during the force−distance cycles, observing an exponentially increase of the unbinding frequency with the contact time, until the reaching of a plateau. This has allowed us to find $t_{0.5} \sim 0.06$ s and then $k_{on} = 1.5 \times 10^4$ $M^{-1}s^{-1}$. Since the ratio between the dissociation and association rate constants defines the dissociation constant, $K_d = k_{off}/k_{on}$, we have then estimated $K_d = 6 \times 10^{-6}$ M, such a value being indicative of a significant stability of the p53−azurin complex. On the other hand, experiments performed in bulk have estimated a lower K_d value (about 33 nM).[113] Such a discrepancy could be attributed to the overestimation of k_{off} by the Bell−Evans model and/or to an underestimation of k_{on}, likely due to the contribution of nonspecific or multiple events.

p53−Mdm2−Azurin: Kinetics and Competition by AFS

The activity of p53 is down-regulated by the cellular oncoprotein Mdm2 that promotes the ubiquitin-dependent degradation of p53, inhibiting its transcriptional function through the formation of a complex with the N-terminal part of p53.[114,115] Accordingly, we have investigated the interaction properties between p53 and Mdm2. In addition, we have explored the appealing hypothesis that azurin could compete with Mdm2 for the complex formation with p53, contrasting then the negative regulation exerted by Mdm2. With such an aim, we have studied the p53−Mdm2−azurin ternary complex.

The immobilization architecture used to study the p53−Mdm2 interaction is shown in Figure 15. The p53 has been anchored

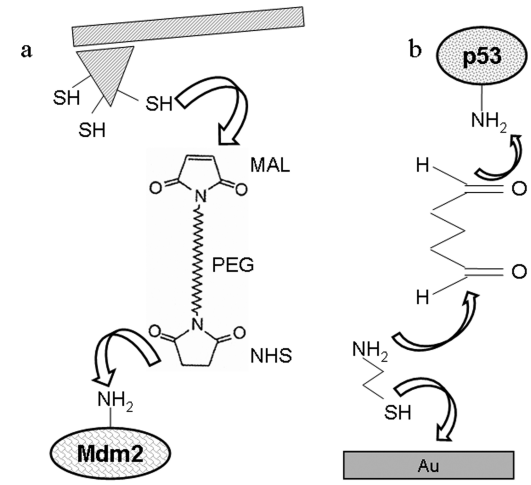

Figure 15. Schematic illustration of the immobilization strategy used for studying the unbinding process of the p53−Mdm2 complex. Mdm2 is anchored to the tip through a PEG spacer binding its lysines. The p53 is bound to a gold substrate by a short spacer binding its lysines.

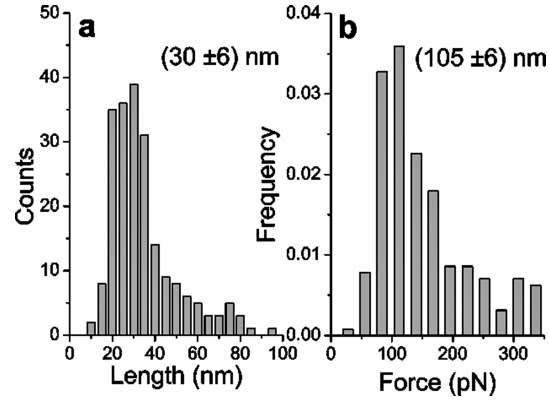

Figure 16. (a) Unbinding length and (b) unbinding force distributions for the p53−mdm2 complex, immobilized through the strategy shown in Figure 15. The force curves have been recorded at the nominal loading rate of 3 nN/s. The extracted central values of the fitted Gaussian distributions and the related statistical errors, obtained by $2\sigma/N^{1/2}$ for a 95.4% confidence level, are reported.

to a gold substrate via cysteamine−glutaraldehyde, and Mdm2 has been bound to the tip by means of a 30 nm long PEG linker which targets the lysine residues of the protein. The use of this longer flexible linker to bind Mdm2 would help to better distinguish between specific and nonspecific interactions according to the previous results[76,99] and would provide Mdm2 with reorientational freedom and mobility to compensate for the somewhat restricted mobility of p53 molecules.

AFS force curves have been analyzed by the same criteria applied in the previous cases. The distributions of the unbinding lengths and forces, at the nominal loading rate of 3 nN/s, are shown in Figure 16a and b, respectively. The unbinding length distribution is constituted by a quite broad single peak centered at around 30 nm. Accordingly, we have therefore selected unbinding events as being specific when they occurred at an unbinding length higher than 30 nm.

The unbinding force histogram is asymmetric and somewhat spread; again a skew toward high force values is observed. In this respect, analogous considerations can be made about the contribution from multiple events and from the variability in the binding processes in order to justify the deviation from the Bell−Evans model. The most probable force has been found to be about 105 nN.

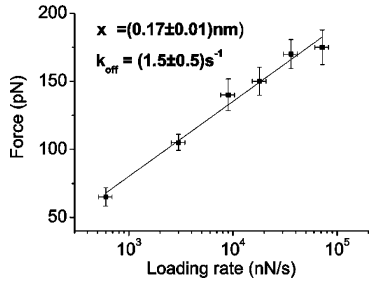

Figure 17. The most probable unbinding force dependence on the logarithm of the loading rate for the p53−Mdm2 complex. Errors on the unbinding force have been derived from the standard deviation of the related distribution. Errors on the loading rate, $R = k_{sys}v$, have been evaluated by the error propagation, where the error of k_{sys} has been estimated as the uncertainty in the slope of the retraction curve while the errors on v have been derived from experimental apparatus. The solid line is a numerical fit of the experimental data to the Bell−Evans model (eq 9); the extracted parameters are reported.

The unbinding frequency has been found to be 18 ± 3% for a set of four experiments performed under the same conditions. The specificity of the observed events has been checked by different blocking experiments. In the first one, we have incubated the p53-functionalized substrate with a solution of Mdm2, while in a second experiment, the Mdm2-functionalized tip has been incubated with a solution of p53. In both cases, we have observed a reduction of the unbinding frequency of more than 60%. Very likely, the observed events can be put into relationship with the formation of a complex between these two proteins.

By plotting the measured rupture forces versus the logarithm of the loading rate, we have obtained a linear relation between the two quantities, as shown in Figure 17, this being indicative of a single energy barrier in the energy profile in the Bell−Evans framework. Accordingly, we have estimated a k_{off} of 1.5 s^{-1} and x_β of 0.17 nm. The k_{off} is close to the value reported for the interaction between the N-terminal portion of p53 and Mdm2.[116] Moreover, the k_{off} is higher than that observed for the p53−azurin complex; this is probably consistent with the different roles played by Mdm2 and azurin in the interaction with p53.

We then investigated the possible role of azurin in competing with Mdm2 for binding p53 by using two different procedures, schematically shown in Figure 18. We first measured the unbinding frequency between a p53-functionalized substrate and an azurin-functionalized tip (Figure 18a, left). Here, the tip was prepared by following the same strategy used to produce Mdm2-functionalized tips. In this way, the unbinding frequency resulted to be around 14% and thus a little bit lower in comparison to the 19% found in the previous experiments in which we have investigated the p53−azurin interaction. However, it has to be reminded that in those studies, azurin was specifically oriented with the hydrophobic patch facing p53 molecules. The PEG used here, at variance, binds the lysine residues of azurin, causing a random orientation that justifies the reduced unbinding frequency. When the p53 sample has been blocked with an azurin solution, the force curves recorded with the azurin-functionalized tip have shown a dramatic reduction of the unbinding frequency, confirming the specificity of the interaction between p53 and azurin (Figure 18a, right).

Then, we incubated the p53 sample with a solution containing Mdm2 molecules (Figure 18b, left). Under these conditions, the frequency of interaction between p53 and azurin remained substantially unchanged (Figure 18b, right). A difference of 2% is within the variability commonly observed in the unbinding frequency measurements.

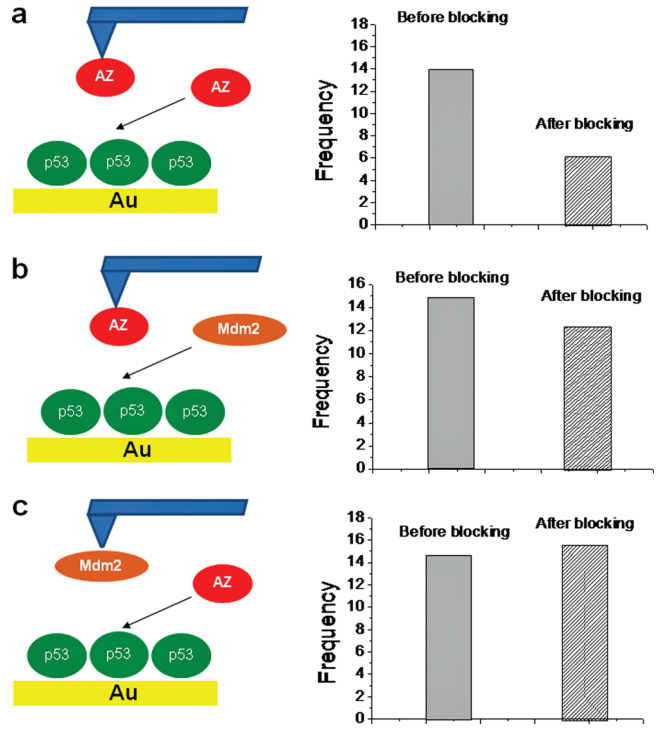

Figure 18. Experiments testing the competition between azurin and Mdm2 for binding p53. (a) Schematic illustration of the control system used to investigate azurin as a competitor for the p53−azurin complex (left); the corresponding unbinding frequencies are observed before (solid) and after (dashed) the azurin deposition (right). (b) Schematic illustration of the system used to investigate Mdm2 as a competitor for the p53−azurin complex (left); the corresponding unbinding frequencies are observed before (solid) and after (dashed) the Mdm2 deposition (right). (c) Schematic illustration of the system used to investigate azurin as a competitor for the p53−Mdm2 complex (left); the corresponding unbinding frequencies are observed before (solid) and after (dashed) the azurin deposition (right).

To validate this result, a blocking procedure has been used to investigate the possibility of a competition between azurin and Mdm2 (Figure 18c, left). Accordingly, the frequency of interaction between a p53 sample and a Mdm2-functionalized tip has been measured before and after adding an azurin solution on the p53 sample. The unbinding between p53 and Mdm2 has resulted in not being affected by the presence of azurin (Figure 18c, right). The results suggest that azurin and Mdm2 interact with two different regions of p53 and form a ternary complex. The occurrence of a p53−Mdm2−azurin ternary complex opens a possible new scenario for the anticancer action of azurin by also providing evidence that AFS offers a valid tool for the study ternary complexes at single-molecule level. Docking computational studies could be useful to plan new, additional AFS experiments to get more insight into the ternary complex involving p53, azurin, and Mdm2.

Conclusions and Outlooks

During the past two decades, single-molecule techniques have undergone rapid development and continuous refinements, becoming powerful tools to gain deep insights into the biological nanoworld. In particular, the success of single-molecule AFS is witnessed by both the number of scientific publications that have continually increased in the latest years and the hundreds of atomic force microscopes devoted to AFS studies in the worldwide scientific community. Since AFS allows one to observe biological systems in near-physiological conditions, at the single-molecule

level, and without altering them by labeling procedures, it is by now routinely used to reach a deeper knowledge, complementing more traditional biomolecular approaches.

By revisiting our AFS works and within a wider context of literature, we have provided a critical analysis on how the AFS technique can be reliably applied to study biological complexes and also in the perspective to extract significant information on the kinetic and thermodynamic aspects which are often hidden in bulk measurements. Furthermore, we have emphasized the use of AFS to investigate not only individual molecular complexes with different affinities but also competitive binding mechanisms among different ligands, thus gaining new insights into molecular interactions.

Besides the undoubted successes of AFS in studying biomolecular systems, some crucial related experimental and theoretical issues which are still widely debated have been outlined. First, the choice of the strategy to anchor biomolecules to the solid, inorganic surfaces (tip or substrates) has been demonstrated to have a high impact on the measured parameters (the unbinding force, the dissociation rate k_{off}, and the energy barrier width x_β). In fact, the kind of immobilization may strongly affect the protein functionality, the capability of partners to recognize each other, the chance of obtaining single interactions, and also the possibility to distinguish true complex dissociations from nonspecific events. Direct, practical evidence of these effects has been provided by the analysis of three different biological systems. In this respect, although a well-defined immobilization strategy susceptible to be adopted in all of the investigated systems has not been so far established, there is a general consensus on some indispensable requirements to be satisfied. For instance, the introduction of spacers, providing a strong, covalent attachment of the biomolecules to the surface and keeping biomolecules from direct contact with the inorganic substrate, should be strongly recommended. On the other hand, the use of long, flexible linkers to immobilize both of the partners is necessary to provide the required reorientational freedom to favor the biorecognition process and, at the same time, to discriminate specific from nonspecific unbinding events. It has been noted in passing that a valid support to design appropriate biomolecule immobilization procedures may be represented by computational docking, which allows one to predict the most probable configuration of molecular complexes when the interaction sites of the partners are unknown. Such an approach, offering the possibility to integrate AFS data with the knowledge of the system at the molecular level, could also allow a more detailed description of the unbinding mechanisms.

In an AFS experiment, special attention should be paid to the selection of those force curves which can arise from specific unbinding events. Such an analysis may take advantage of both the expected and measured stretching features of the linkers and of blocking experiments suitably conceived.

The extraction of equilibrium parameters from nonequilibrium AFS experiments requires the application of appropriate theoretical models. We have outlined that the most widely used Bell−Evans model, which relies on some rather restrictive assumptions (such as the occurrence of single unbinding events, a constant loading rate, and so forth) provides a satisfactorily description of the AFS data for several biological systems, even if some discrepancies in the extracted parameter values have been recently put into evidence. The Bell−Evans model predicts a linear relationship between the most probable unbinding force and the logarithm of the loading rate, and it allows one to extract the dissociation rate k_{off} and the energy barrier width x_β of the unbinding process. In this respect, the most probable unbinding force should be evaluated from the experimental distributions of the unbinding forces recorded at a given loading rate. These distributions, often characterized by an asymmetric shape, are commonly fitted by single or multiple Gaussian distributions. However, since these fits can neglect the contribution of higher force values, they can introduce systematic errors into the analysis. Additionally, special attention has to be devoted to evaluate the loading rate effectively applied to the system in order to avoid the introduction of artifacts which may significantly affect the final results. On the other hand, new theoretical models, able to provide a more consistent interpretation of the experimental data, even overcoming some of the drawbacks of the Bell−Evans model, have been developed. It could be however desirable to have new models which, providing a more general description of the unbinding processes, also allow one to disclose, at a deeper level, the mechanisms regulating biological interactions. In this respect, we mention the applications of innovative theoretical tools, such as the Jarzynszi's equality, which make possible the extraction of equilibrium properties from measurements performed away from equilibrium, allowing reconstruction of the entire equilibrium energy landscape of single-molecule processes.[117,118]

Finally, it should be noted that the possibility of probing individual systems makes AFS ideal for cutting edge applications, such as the development of nanobiosensors, even for medical and pharmaceutical aims, for example, drug screening. A significant improvement along this direction may arise from the parallel detection by means of multiple cantilevers differently functionalized. In the near future, AFS will surely benefit of AFM equipment with further, advanced capabilities. Very low drift AFMs will permit one to follow biological processes, such as ligand−receptor binding or unbinding processes, for longer times in order to access near-equilibrium conditions.[117] Development of high-speed AFM techniques will be suitable to elucidate fast biological events in real time. Furthermore, AFS combined with fast AFM imaging will give a boost in the acquisition biomolecular information due to the capability of simultaneous monitoring of biorecognition events and topological features.[119]

The combination of force spectroscopy with other advanced techniques will lead to the development of multisensing approaches able to provide a broader view on the complexity of biological systems. For example, the use of gold supports opens the possibility of investigating, at the level of single molecules, both the biorecognition capability of immobilized proteins by AFS and their conductive properties by scanning tunneling microscopy (STM) or conductive AFM, with interesting new perspectives in ultrasensitive detection.[120]

Acknowledgment. We would like to thank Monia Taranta for her help in the preliminary draft of the manuscript and Gloria Funari for generating Figs 15 and 18.

References and Notes

(1) Engel, A.; Muller, D. *Nat. Struct. Biol.* **2000**, *7*, 715–718.
(2) Scheuring, S.; Sturgis, J. N. *Science* **2005**, *309*, 484–487.
(3) van Holde, K.; Zlatanova, J. *Semin. Cell Dev. Biol.* **2007**, *18*, 651–658.
(4) Mysiak, M. E.; Bleijenberg, M. H.; Wyman, C.; Holthuizen, P. E.; van der Vliet, P. C. *J. Virol.* **2004**, *78*, 1928–1935.
(5) Maurer, S.; Fritz, J.; Muskhelishvili, G.; Travers, A. *EMBO J.* **2006**, *25*, 3784–90.
(6) Tessmer, I.; Moore, T.; Lloyd, R. G.; Wilson, A.; Erie, D. A.; Allen, S.; Tendler, S. J. B. *J. Mol. Biol.* **2005**, *350*, 254–262.
(7) Jiao, Y.; Cherny, D. I.; Heim, G.; Jovin, T. M.; Schaffer, T. E. *J. Mol. Biol.* **2001**, *314*, 233–243.
(8) Danker, T.; Oberleithner, H. *Pflugers Arch.* **2000**, *439*, 671–81.

(9) Ando, T.; Uchihashi, T.; Kodera, N.; Yamamoto, D.; Miyagi, A.; Taniguchi, M.; Yamashita, H. *Pflugers Arch.* **2008**, *456*, 211–225.
(10) Lee, G. U.; Kidwell, D. A.; Colton, R. J. *Langmuir* **1994**, *10*, 354–357.
(11) Florin, E. L.; Moy, V. T.; Gaub, H. E. *Science* **1994**, *264*, 415–417.
(12) Moy, V. T.; Florin, E. L.; Gaub, H. E. *Science* **1994**, *266*, 257–259.
(13) Hugel, T.; Grosholz, M.; Clausen-Schaumann, H.; Pfau, A.; Gaub, H.; Seitz, M. *Macromolecules* **2001**, *34*, 1039–1047.
(14) Cross, S. E.; Jin, Y. S.; Rao, J.; Gimzewski, J. K. *Nat. Nanotechnol.* **2007**, *2*, 780–783.
(15) Rief, M.; Oesterhelt, F.; Heymann, B.; Gaub, H. *Science* **1997**, *276*, 1109–1112.
(16) Muller, D. J.; Baumeister, W.; Engel, A. *Proc. Natl. Acad. Sci. U.S.A.* **1999**, *96*, 13170–13174.
(17) Ros, R.; Schwesinger, F.; Anselmetti, D.; Kubon, M.; Schafer, R.; Pluckthun, A.; Tiefenauer, L. *Proc. Natl. Acad. Sci. U.S.A.* **1998**, *95*, 7402–7405.
(18) Sulchek, T. A.; Friddle, R. W.; Langry, K.; Lau, E. Y.; Albrecht, H.; Ratto, T. V.; DeNardo, S. J.; Colvin, M. E.; Noy, A. *Proc. Natl. Acad. Sci. U.S.A.* **2005**, *102*, 16638–16643.
(19) Taranta, M.; Bizzarri, A. R.; Cannistraro, S. *J. Mol. Recognit.* **2008**, *21*, 63–70.
(20) Merkel, R.; Nassoy, P.; Leung, A.; Ritchie, K.; Evans, E. *Nature* **1999**, *397*, 50–53.
(21) Evans, E.; Ritchie, K. *Biophys. J.* **1997**, *72*, 1541–1555.
(22) Bell, G. I. *Science* **1978**, *200*, 618–627.
(23) Hinterdorfer, P.; Dufrêne, Y. F. *Nat. Methods* **2006**, *5*, 347–355.
(24) Bonanni, B.; Andolfi, L.; Bizzarri, A. R.; Cannistraro, S. *J. Phys. Chem. B* **2007**, *111*, 5062–5075.
(25) Willemsen, O. H.; Snel, M. M. E.; van der Werf, K. O.; de Grooth, B. G.; Greve, J.; Hinterdorfer, P.; Gruber, H. J.; Schindler, H.; van Kooyk, Y.; Figdor, C. G. *Biophys. J.* **1998**, *75*, 2220–2228.
(26) Dudko, O. K.; Filippov, A. E.; Klafter, J.; Urbakh, M. *Proc. Natl. Acad. Sci. U.S.A.* **2003**, *100*, 11378–11381.
(27) Dudko, O. K.; Hummer, G.; Szabo, A. *Phys. Rev. Lett.* **2006**, *96*, 108101−1-4.
(28) Hummer, G.; Szabo, A. *Biophys. J.* **2003**, *85*, 5–15.
(29) Bonanni, B.; Kamruzzahan, A. S. M.; Bizzarri, A. R.; Rankl, C.; Gruber, H. J.; Hinterdorfer, P.; Cannistraro, S. *Biophys. J.* **2005**, *89*, 2783–2791.
(30) Bonanni, B.; Bizzarri, A. R.; Cannistraro, S. *J. Phys. Chem. B* **2006**, *110*, 14574–14580.
(31) Funari, G.; Domenici F.; Nardinocchi, L.; Puca, R.; D'Orazi, G.; Bizzarri, A. R.; Cannistraro, S. *J. Mol. Recognit.* In press.
(32) Schlosshauer, M.; Baker, D. *Protein Sci.* **2004**, *13*, 1660–1669.
(33) Robert, P.; Benoliel, A. M.; Pierres, A.; Bongrand, P. *J. Mol. Recognit.* **2007**, *20*, 432–447.
(34) Schwesinger, F.; Ros, R.; Strunz, T.; Anselmetti, D.; Guntherodt, H.-J.; Honegger, A.; Jermutus, L.; Tiefenauer, L.; Pluckthun, A. *Proc. Natl. Acad. Sci. U.S.A.* **2000**, *97*, 9972–9977.
(35) Eccleston, J. F.; Martin, S. R.; Schilstra, M. J. *Methods Cell Biol.* **2008**, *84*, 445–477.
(36) Tanious, F. A.; Nguyen, B.; Wilson, W. D. *Methods Cell Biol.* **2008**, *84*, 53–77.
(37) Andreev, I. A.; Hyon Kim, S.; Kalinina, N. O.; Rakitina, D. V.; Fitzgerald, A. G.; Palukaitis, P.; Taliansky, M. E. *J. Mol. Biol.* **2004**, *339*, 1041–1047.
(38) Nevo, R.; Stroh, C.; Kienberger, F.; Kaftan, D.; Brumfeld, V.; Elbaum, M.; Reich, Z.; Hinterdorfer, P. *Nat. Struct. Biol.* **2003**, *10*, 553–55787.
(39) Zepeda, S.; Yeh, Y.; Noy, A. *Langmuir* **2003**, *19*, 1457–1461.
(40) Rico, F.; Moy, V. T. *J. Mol. Recognit.* **2007**, *20*, 495–501.
(41) Heymann, B.; Grubmueller, H. *Phys. Rev. Lett.* **2000**, *84*, 6126–6129.
(42) Vestweber, D.; Blanks, J. E. *Physiol. Rev.* **1999**, *79*, 181–213.
(43) De Paris, R.; Strunz, T.; Oroszlan, K.; Guntherodt, H.-J.; Hegner, M. *Single Mol.* **2000**, *4*, 285–290.
(44) Yuan, C.; Chen, A.; Kolb, P.; Moy, V. T. *Biochemistry* **2000**, *39*, 10219–10223.
(45) Hinterdorfer, P.; Baumgartner, W.; Gruber, H. J.; Schilcher, K.; Schindler, H. *Proc. Natl. Acad. Sci. U.S.A.* **1996**, *93*, 3477–3481.
(46) Berquand, A.; Xia, N.; Castner, D. G.; Clare, B. H.; Abbott, N. L.; Dupres, V.; Adriaensen, Y.; Dufrene, Y. F. *Langmuir* **2005**, *21*, 5517–5523.
(47) Fritz, J.; Katopodis, A. G.; Kolbinger, F.; Anselmetti, D. *Proc. Natl. Acad. Sci. U.S.A.* **1998**, *95*, 12283–12288.
(48) Almqvist, N.; Bhatia, R.; Primbs, G.; Desai, N.; Banerjee, S.; Lal, S. *Biophys. J.* **2004**, *86*, 1753–1762.
(49) Eckel, R.; Wilking, S. D.; Becker, A.; Norbert Sewald, N.; Ros, R.; Anselmetti, D. *Angew. Chem., Int. Ed.* **2005**, *44*, 3921–3924.
(50) Kuhner, F.; Costa, L. T.; Bisch, P. M.; Thalhammer, S.; Heckl, W. M.; Gaub, H. E. *Biophys. J.* **2004**, *87*, 2683–2690.
(51) Krasnoslobodtsev, A. V.; Shlyakhtenko, L. S.; Lyubchenko, Y. L. *J. Mol. Biol.* **2007**, *365*, 1407–1416.
(52) Vinckier, A.; Gervasoni, P.; Zaugg, F.; Ziegler, U.; Lindner, P.; Groscurth, P.; Pluckthun, A.; Semenza, G. *Biophys. J.* **1998**, *74*, 3256–3263.
(53) Garcia-Manyes, S.; Bucior, I.; Ros, R.; Anselmetti, D.; Sanz, F.; Burger, M. M.; Fernandez-Busquets, X. *J. Biol. Chem.* **2006**, *281*, 5992–5999.
(54) Dague, E.; Alsteens, D.; Latge, J.-P.; Verbelen, C.; Raze, D.; Baulard, A. R.; Dufrene, Y. F. *Nano Lett.* **2007**, *7*, 3026–3030.
(55) Lee, A. S.; Mahapatro, M.; Caron, D. A.; Requicha, A. A.; Stauffer, B. A.; Thompson, M. E.; Zhou, C. *IEEE Trans. Nanobiosci.* **2006**, *5*, 149–156.
(56) Synder, P. W.; Lee, G.; Marszalek, P. E.; Clark, R. L.; Toone, E. J. *Proc. Natl. Acad. Sci. U.S.A.* **2007**, *104*, 2579–2584.
(57) Raible, M.; Evstigneev, M.; Bartels, F. W.; Eckel, R.; Nguyen-Duong, M.; Merkel, R.; Ros, R.; Anselmetti, D.; Reimann, P. *Biophys. J.* **2006**, *90*, 3851–3864.
(58) Strunz, T.; Oroszlan, K.; Schafer, R.; Guntherodt, H. J. *Proc. Natl. Acad. Sci. U.S.A.* **1999**, *96*, 11277–11282.
(59) Baumgartner, W.; Hinterdorfer, P.; Ness, W.; Raab, A.; Vestweber, D.; Schindler, H.; Drenckhahn, D. *Proc. Natl. Acad. Sci. U.S.A.* **2000**, *97*, 4005–4010.
(60) Morfill, K.; Blank, C.; Zahnd, B.; Luginbuhl, F.; Kuhner, K. E.; Gottschalk, A.; Pluckthun, H.; Gaub, E. *Biophys. J.* **2007**, *93*, 3583–3590.
(61) Pincet, F.; Husson, J. *Biophys. J.* **2005**, *89*, 4374–4381.
(62) Friedsam, C.; Wehle, A. K.; Kuhner, F.; Gaub, H. E. *J. Phys.: Condens. Matter* **2003**, *15*, S1709-S1723.
(63) Williams, P. M. *Anal. Chim. Acta* **2003**, *479*, 107–115.
(64) Hammer, D.; Apte, S. *Biophys. J.* **1992**, *63*, 35–57.
(65) Friddle, R. W. *Phys. Rev. Lett.* **2008**, *100*, 138302/1−138302/4.
(66) Dudko, O. K.; Hummer, G.; Szabo, A. *Proc. Natl. Acad. Sci. U.S.A.* **2008**, *105*, 15755–15760.
(67) Ulman, A. *Chem. Rev.* **1996**, *96*, 1533–1554.
(68) Dettmann, W.; Grandbois, M.; André, S.; Benoit, M.; Wehle, A. K.; Kaltner, H.; Gabius, H. J.; Gaub, H. E. *Arch. Biochem. Biophys.* **2000**, *383*, 157–170.
(69) Wong, J.; Chilkoti, A.; Moy, V. T. *Biomol. Eng.* **1999**, *16*, 45–55.
(70) Schumakovitch, I.; Grange, W.; Strunz, T.; Bertoncini, P.; Guntherodt, H. J.; Hegner, M. *Biophys. J.* **2002**, *82*, 517–521.
(71) Odorico, M.; Teulon, J. M.; Bessou, T.; Vidaud, C.; Bellanger, L.; Chen, S. W.; Quéméneur, E.; Parot, P.; Pellequer, J. L. *Biophys. J.* **2007**, *93*, 645–654.
(72) Dammer, U.; Hegner, M.; Anselmetti, D.; Wagner, P.; Drier, M.; Huber, W.; Guntherodt, H.-J. *Biophys. J.* **1996**, *70*, 2437–2441.
(73) Allen, S.; Chen, X.; Davies, J.; Davies, M. C.; Dawkes, A. C.; Edwards, J. C.; Roberts, O. J.; Sefton, J.; Tendler, S. J. B.; Williams, P. M. *Biochemistry* **1997**, *36*, 7457–7463.
(74) Yip, C. M.; Yip, C. C.; Ward, M. D. *Biochemistry* **1998**, *37*, 5439–5449.
(75) Yoshimura, S. H.; Takahashi, H.; Otsuka, S.; Takeyasu, K. *FEBS Lett.* **2006**, *580*, 3961–3965.
(76) Ratto, T. V.; Langry, K. C.; Rudd, R. E.; Balhorn, R. L.; Allen, M. J.; McElfresh, M. W. *Biophys. J.* **2004**, *86*, 2430–2437.
(77) Wang, T.; Ikai, A. *Jpn. Appl. Phys.* **1999**, *38*, 3912–3917.
(78) Wong, S. S.; Joselevich, E.; Woolley, A. T.; Cheung, C. L.; Lieber, C. M. *Nature.* **1998**, *394*, 52–55.
(79) Yoshimura, S. H.; Takahashi, H.; Otsuka, S.; Takeyasu, K. *FEBS Lett.* **2006**, *580*, 3961–3965.
(80) Y. Gilbert, Y.; Deghorain, M.; Wang, L.; Xu, B.; Pollheimer, P. D.; Gruber, H. J.; Errington, J.; Hallet, B.; Haulot, X.; Verbelen, C.; Hols, P.; Dufrêne, Y. F. *Nano Lett.* **2007**, *7*, 796–801.
(81) Sulchek, T. A.; Friddle, R. W.; Noy, A. *Biophys. J.* **2006**, *90*, 4686–4691.
(82) Xu, S.; Dong, M.; Liu, X.; Howard, K. A.; Kjems, J.; Besenbacher, F. *Biophys. J.* **2007**, *93*, 952–959.
(83) Yadavalli, V. K.; Forbes, J. G.; Wang, K. *Langmuir* **2006**, *22*, 6969–6976.
(84) Bizzarri, A. R.; Costantini, G.; Bonanni, B.; Cannistraro, S. *ChemPhysChem* **2003**, *4*, 1189–1195.
(85) Jones, S.; Thornton, J. M. *Proc. Natl. Acad. Sci. U.S.A.* **1996**, *93*, 13–20.
(86) De Grandis, V.; Bizzarri, A. R.; Cannistraro, S. *J. Mol. Recognit.* **2007**, *20*, 215–226.
(87) Taranta, M.; Bizzarri, A. R.; Cannistraro, S. *J. Mol. Recognit.* **2009**, *15*, 15–22.
(88) Hutter, J. L.; Bechhoefer, J. *Rev. Sci. Instrum.* **1993**, *64*, 1868–1873.
(89) Sader, J. E.; Chon, J. W. M.; Mulvaney, P. *Rev. Sci. Instrum.* **1999**, *70*, 3967–3969.
(90) Heinz, W. F.; Hoh, J. H. *Trends Biotechnol.* **1999**, *17*, 143–150.

(91) Zlatanova, J.; Lindsay, S. M.; Leuba, S. H. *Prog. Biophys. Mol. Biol.* **2000**, *74*, 37–71.
(92) Marzsalek, P. E.; Oberhauser, A. F.; Pang, Y. P.; Fernandez, J. M. *Nature* **1998**, *396*, 661–664.
(93) Gu, S.; Ray, C.; Kirkpatrick, A.; Lad, N.; Akhremitchev, B. B. *Biophys. J.* **2008**, *95*, 3964.
(94) Ray, C.; Akhremitchev, B. B. *J. Am. Chem. Soc.* **2005**, *127*, 14739–14744.
(95) Kienberger, F.; Pastushenko, V. P.; Kada, G.; Gruber, H. J.; Riener, C.; Schindler, H.; Hinterdorfer, P. *Single Mol.* **2000**, *1*, 123–128.
(96) Bouchiat, C.; Wang, M. D.; Allemand, J.-F.; Strick, T.; Block, S. M.; Croquette, V. *Biophys. J.* **1999**, *76*, 409–413.
(97) Oesterhelt, F.; Rief, M.; Gaub, H. E. *New J. Phys.* **1999**, *1*, 1–11.
(98) Kamper, S. G.; Porter-Peden, L.; Blankespoor, R.; Sinniah, K.; Zhou, D.; Abell, C.; Rayment, T. *Langmuir* **2007**, *23*, 12561–12565.
(99) Ray, C.; Brown, J. R.; Akhremitchev, B. B. *J. Phys. Chem. B* **2007**, *111*, 1963–1974.
(100) Perret, E.; Leung, A.; Feracci, H.; Evans, E. *Proc. Natl. Acad. Sci. U.S.A.* **2004**, *101*, 16472–16477.
(101) Shi, Q.; Chien, J. H.; Leckband, D. *J. Biol. Chem.* **2008**, *28*, 28454–28463.
(102) Fuhrmann, A.; Anselmetti, D.; Ros, R. *Phys. Rev. E* **2008**, *77*, 031912−1-10.
(103) Cutruzzolà, F.; Arese, M.; Ranghino, G.; van Pouderoyen, G.; Canters, G. W.; Brunori, M. *J. Inorg. Biochem.* **2002**, *88*, 353–361.
(104) Andolfi, L.; Bizzarri, A. R.; Cannistraro, S. *Thin Solid Films* **2006**, *515*, 212–219.
(105) Vakser, I. A.; Matar, O. G.; Lam, C. F. *Proc. Natl. Acad. Sci. U.S.A.* **1999**, *84*, 77–8482.
(106) Bizzarri, A. R.; Brunori, E.; Bonanni, B.; Cannistraro, S. *J. Mol. Recognit.* **2007**, *20*, 122–131.
(107) Nar, H.; Messerschmidt, A.; Huber, R.; van de Kamp, M.; Canters, G. W. *J. Mol. Biol.* **1991**, *218*, 427–447.
(108) Crowley, P. B.; Ubbink., M. *Acc. Chem. Res.* **2003**, *36*, 723–730.
(109) Yamada, T.; Goto, M.; Punj, V.; Zaborina, O.; Kimbara, K.; Das Gupta, T. K.; Chakrabarty, A. M. *Infect. Immun.* **2002**, *70*, 7054–7062.
(110) Goto, M.; Yamada, T.; Kimbara, K.; Horner, J.; Newcomb, M.; Das Gupta, T. K.; Chakrabarty, A. M. *Mol. Microbiol.* **2003**, *47*, 549–559.
(111) Chen, R.; Weng, Z. *Proteins: Struct., Funct., Genet.* **2003**, *51*, 397–408.
(112) Punj, V.; Das Gupta, T. K.; Chakrabarty, A. M. *Biochem. Biophys. Res. Commun.* **2003**, *312*, 109–114.
(113) Apiyo, D.; Wittung-Stafshede, P. *Biochem. Biophys. Res. Commun.* **2005**, *332*, 965–968.
(114) Shon, O.; Friedler, A.; Bycroft, M.; Freund, S. M. V.; Fersht, A. R. *J. Mol. Biol.* **2002**, *323*, 491–501.
(115) Honda, R.; Tanaka, H.; Yasuda, H. *FEBS Lett.* **1997**, *420*, 25–27.
(116) Junker, J. P.; Ziegler, F.; Rief, M. *Science* **2009**, *323*, 633–637.
(117) Jarzynski, C. *Phys. Rev. Lett.* **1997**, *78*, 2690–2694.
(118) Hummer, G.; Szabo, A. *Acc. Chem. Res.* **2005**, *38*, 504–513.
(119) Ebner, A.; Kienberger, F.; Kada, G.; Stroh, C. M.; Geretschläger, M.; Kamruzzahan, A. S. M.; Wildling, L.; Johnson, W. T.; Ashcroft, B.; Nelson, J.; Lindsay, S. M.; Gruber, H. J.; Hinterdorfer, P. *ChemPhysChem* **2005**, *6*, 897–900.
(120) Choi, J. W.; Oh, B. K.; Jang, Y. H.; Kang, D. Y. *Appl. Phys. Lett.* **2008**, *93*, 033110/1−033110/3.

JP902421R